Journal of Hydrology 631 (2024) 130860

Contents lists available at ScienceDirect

Journal of Hydrology

journal homepage: www.elsevier.com/locate/jhydrol

Research papers

Advanced type curves for vertical groundwater flow estimation from temperature profiles. Applications to real scenarios

José Antonio Jiménez-Valera [a], Iván Alhama [a,*], Carlos Duque [b,c]

[a] Mining and Civil Engineering Department, Technical University of Cartagena, Paseo Alfonso XIII, n° 52 – 30203, Cartagena, Spain
[b] Department of Geodynamics, University of Granada, Av. Fuentenueva s/n Granada, Spain
[c] Department of Geosciences, University of Oslo, Sem Sælands vei 1, 0371 Oslo, Norway

ARTICLE INFO

This manuscript was handled by Corrado Corradini, Editor-in-Chief, with the assistance of William Payton Gardner, Associate Editor

Keywords:
Groundwater flow
Temperature-depth profiles
Inverse problem
Dimensionless groups
Heat transfer
Porous media

ABSTRACT

Groundwater discharge or recharge in aquifers can be obtained from the analysis of temperature profiles, a cost-efficient method widely applied in hydrogeology. In this study we proposed a set of type curves that can be used for estimating the vertical velocity flow, and have the potential to allow, in certain cases, the assessment of the thermal diffusivity of the soil matrix. The solutions, represented graphically, establish the dependencies of the basic parameters involved in the process: groundwater velocity, thermal conductivity, specific heat, aquifer depth and harmonic temperature period. Using the non-dimensionalization technique, the mentioned parameters were organized in dimensionless groups which are verified by numerical simulations. For the estimates of the groundwater velocity, transient temperature-depth measurements or steady state amplitudes of the harmonic oscillation were used as input data. In this last case, a particular type curve solution allows us to assess the depth from which temperature oscillations have a negligible amplitude compared to the amplitude at the ground surface. The resulting dependencies have been applied to estimate the groundwater velocity in real aquifers and laboratory experiences.

1. Introduction and background

The use of temperature to estimate water velocity in aquifers as a cost efficient method has been studied for several decades (Cartwright, 1979; Anderson, 2005; Keery et al., 2007). In saturated aquifers, groundwater flow with vertical upward or downward velocity components, the problem of heat transfer caused by temperature boundary conditions has been a topic of great interest in hydrogeology because of the possibility of determining recharge or discharge flows between shallow and deep bodies of water using temperature-depth profiles, as well as other mechanical or thermal soil properties (Silliman et al., 1995; Hatch et al., 2002; Ferguson and Woodbury, 2005).

In this section and in order to highlight the contribution of present work, we run through the main references in this field to summarize the key ideas and applicability. After that, we present the methodology carried out and the results. Finally, and aimed to put into practice and better understand the main contribution, the results have been applied to two real scenarios previously studied by other authors.

Especially in the context of study groundwater-surface water interaction, the use of temperature profiles has been applied in recent years to estimate groundwater discharge (Sebok et al., 2013; Duque et al., 2016). The use of analytical solutions to determine groundwater discharge provides rapid estimation of flows that would otherwise require extensive field campaigns, or modeling efforts for which additional field data are also needed. However, several important uncertainties concerning assumptions such as steady water flow with a vertical-only component or aquifers with homogeneous thermal properties could deviate the measured temperature profiles from those supposedly expected.

Suzuki (1960) was the first who proposed a 1D solution in semi-confined aquifers, under harmonic boundary conditions for the temperature and constant vertical flow of water. His solution, which considers a sinusoidal temperature boundary condition at the aquifer surface, introduces two empirical parameters. Subsequently, Stallman (1965) worked with Suzuki's solution providing a precise expression for such parameters, to which he attributes the dimension m^{-1}.

Bredehoeft and Papadopulos (1965) simplified the solution proposed by Suzuki (1960) for the case of constant temperature at the surface. They introduced an analytical solution showing the temperature dependence with two dimensionless groups, the relative depth and the equilibrium between advective and diffusive effects. This solution

* Corresponding author.
E-mail addresses: jose.jvalera@upct.es (J.A. Jiménez-Valera), ivan.alhama@upct.es (I. Alhama), cduque@ugr.es (C. Duque).

https://doi.org/10.1016/j.jhydrol.2024.130860
Received 30 May 2023; Received in revised form 10 January 2024; Accepted 24 January 2024
Available online 10 February 2024

Nomenclature

a, b, K, V	constants used by Stallman (1965) (cm^{-1})
C_1	constant
c_e	volumetric heat capacity of the rock-fluid matrix ($Jm^{-3}{}^{\circ}C^{-1}$)
$c_{e,s}$	volumetric heat capacity of sediment ($Jm^{-3}{}^{\circ}C^{-1}$)
$c_{e,w}$	volumetric heat capacity of water ($Jm^{-3}{}^{\circ}C^{-1}$)
H	vertical depth of the aquifer
k_m	heat conductivity of the rock-fluid matrix ($Js^{-1}m^{-1}{}^{\circ}C^{-1}$)
$l^*_{diff-conv}$	vertical length for which diffusion and drag effects have the same order of magnitude in a given time (m)
$l_{z,o}{}^*$	caracteristic lenght (m) from which the oscillations have a negligible amplitude compared to the amplitude of the wave on the soil surface
T	temperature (°C)
T_{av}	mean surface soil temperature (°C)
T_{max}	maximum temperature envelope due to sinusoidal temperature fluctuation
T_{min}	minimum temperature envelope due to sinusoidal temperature fluctuation
T_{ini}	initial soil temperature (°C)
T_o	temperature at the bottom of the domain (°C)
$(T' - z')_{profile}$	vertical dimensionless temperature profiles
t	time (s)
$v_{o,z}$	vertical water flow velocity (m/s)
z	vertical spatial coordinate (m)
α	thermal diffusivity (m^2/s)
α_c	corrected thermal diffusivity coefficient (m^2/s)
ΔT	amplitude due to sinusoidal boundary condition at the soil surface
$(\Delta T)_z$	amplitude at vertical z coordinate
$(\Delta T)_{z=0}$	amplitude of the temperature variation at z = 0
Ψ	refers to an arbitrary function of its arguments (contained in parentheses or square brackets)
λ_o	baseline thermal Conductivity ($Js^{-1}m^{-1}{}^{\circ}C^{-1}$)
π_i	dimensionless group (i = 1,2 …)
$\pi_{l_{z,o}{}^*}$	characteristic length monomial
π_{τ^*}	characteristic time monomial
ρ_e	wet bulk density of the rock-fluid matrix (kgm^{-3})
$\rho_{e,s}$	sediment density (kgm^{-3})
$\rho_{e,w}$	water density (kgm^{-3})
τ_o	sinusoidal wave period (s)
τ^*	characteristic time (s)
$\tau^*_{diff-conv}$	time for which the length traveled by advection is equal to the length traveled by diffusion
[]	delimits a range or interval
~	denotes order of magnitude
'	denotes dimensionless parameter

generates lines with curvatures proportional to vertical flow when the above equilibrium is less than 0.5, the limit for detecting groundwater velocities. The main limitation of this solution is that it is only valid for steady state conditions. For 1D flows, Turcotte and Schubert (1982) provided a solution similar to that of Bredehoeft and Papadopulos (1965) that does not explicitly contain the aquifer depth (H). However, both solutions are the same because they use the same boundary conditions. The parameter H does not appear in Turcotte and Schubert's solution but, instead, there is the temperature at$z = H$which is an alternative information.

Ziagos and Blackwell (1986) presented an aquifer trapped between two impermeable bedrock beds where the advection term is not taken into account. Lapham (1989), based on finite-difference method, provided steady state and transient solution of the governing equation of Stallman (1963), which assumes a variable boundary condition at the surface, applying it to real scenarios in different locations of the USA (Hardwick and New Braintree, Massachusetts, and Dover, New Jersey). Taniguchi (1993), based on the work of Stallman (1965), provided a new set of curves that allows the direct determination of the 1D water velocity from temperature profiles. He studied in Nagaoka Plain (Japan) aquifers generally dedicated to water supply affected by seasonal surface temperature changes, determining vertical flow and hydraulic conductivity by fitting experimental measurements with the set of curves.

Lu and Ge (1996) proposed a 1D heat transfer model to describe the vertical heat flux. A source term is embedded in the governing heat flow equation to account for the horizontal thermal gradient. The application of Bredehoeft and Papadopulos (1965) solution has been directly used in numerous and recent studies that required the assumption of steady state conditions (Jensen and Engesgaard, 2011; Sebok et al., 2013; Duque et al., 2016). In all these studies, temperature profiles were taken at the bed of the surface water body (lake, stream, lagoon) and temperature of the groundwater and of the surface water in that moment were considered constant. Kurylyk et al. (2019) extend the analytical solutions of Bredehoeft and Papadopulos (1965) and Turcotte and Schubert (1982) to problems with a more detailed boundary condition on the soil surface and a more realistic soil temperature profile initial condition. In addition, these authors provide an up-to-date and comprehensive literature review in this field regarding the inverse problem of determining water flux from temperature profiles. On the other hand, they use as bottom boundary condition a Neumann type (constant heat flux), which results in variable bottom temperature solutions for non-zero water flows.

The use of numerical solutions has been also an alternative when it was not possible to simplify the functioning of the system. A specific software for this purpose frequently used has been VS2DHI (Healy and Ronan, 1996; Healy, 2008). Schmidt et al. (2007) considered a harmonic surface temperature of a stream and established as constant the bottom of the aquifer. For the transient solution, they used VS2DHI, while for the solution in the steady state, they applied the solution of Turcotte and Schubert (1982). The use of analytical solutions is often useful in standard and simplified scenarios, but they can be evolved to more complicated scenarios or with more complex boundary conditions (Lin et al., 2022). Numerical solutions are necessary when it is not possible to assume hypotheses such as constant phreatic level, horizontal strata, homogeneous thermal properties, etc. Schmidt et al. (2007), for example, combine the use of analytical and numerical solutions to study an aquifer with harmonic surface temperature and constant temperature at the bottom. For the transient solution, they used VS2DHI (Healy, 2008), while for the solution in the steady state, they applied the solution of Turcotte & Schubert (1982).

Hatch et al. (2006) presented a method for determining streambed seepage rates using thermal data (phase changes and amplitude of temperature variations between pairs of subsurface sensors) from time series. They presented solutions for both phase changes and thermal amplitude changes. To work with the amplitudes, the authors collected series of streambed data, applied frequency bandpass filter to extract signal and calculated amplitude ratio and phase shift time series. Lautz (2012) performed controlled laboratory experiments to explore the accuracy of analytical solutions of the one-dimensional heat transport model to capture the temporal variability of flow through porous media from the propagation of a periodic temperature signal at depth. She used the one-dimensional model of heat transport presented by Hatch et al.

(2006) to quantify the velocity of the water through the sand column for comparison and validation. The 1D heat transport model was implemented with the Vertical Fluid Heat Transfer Solver VFLUX (Gordon et al., 2012). This code estimates fluid flow using analytical solutions, Signal processing techniques and Monte Carlo error analysis modules (Irvine et al., 2015).

As for universal (or type-curves) solutions, the one provided by Bredehoeft and Papadopulos is often used due to its simplicity. However, its application assumes that the boundary condition at the top is of Dirichlet type (first type) and that steady state thermal conditions have been reached. The solution provided by Turcotte and Schubert (1982) is very similar to that of Bredehoeft and Papadopulos (1965), while maintaining the same drawbacks. In contrast to these analytical solutions, in this manuscript we propose a set of new universal solutions for both steady state and transient (assuming constant-temperature condition at the surface) and another set to use the amplitudes of the sine wave at different depths (harmonic boundary condition at the surface).

As for Hatch et al. (2006), one of the drawbacks of their scheme is that, a priori, they do not know the vertical locations at which to locate the temperature gauges, since they do not know the depth from which the temperature amplitude is negligible compared to the amplitude in the streambed surface. With the new equations presented in this work, it is possible to simultaneously obtain the thermal properties and even the depth of the aquifer by means of universal curves. Also, a criterion is provided to determine the depth at which the temperature wave amplitude is negligible compared to that of the ground surface, allowing aquifers to be thermally classified as shallow or deep.

2. Methodology

In this work, a new set of universal solutions for simultaneous fluid flow and heat transport was derived for the problem of vertical flow (upward or downward) of groundwater in aquifers. Such solutions can be divided into two types: those that use mean temperature profiles and those related to sinusoidal wave amplitudes in the aquifer.

The approach used to obtain these curves is based on the search for dimensionless groups, an essential objective of Dimensional Analysis, which govern the solutions to the problem and which allow the unknowns sought to be expressed based on such groups by application of the Pi theorem. This task is accomplished through the non-dimensionalization of the governing equations (Appendix A). The main advantage of using the dimensionless technique is that the resulting groups, in addition to being dimensionless, have a clear physical meaning since they are the direct result of the balance of pairs of terms of the governing equation in the same physical domain. This procedure has been applied in coupled flow and transport problems of similar complexity (Cánovas et al., 2015; Seco-Nicolás et al., 2018; Jiménez-Valera and Alhama, 2022).

The first step is the definition of the governing equation and the boundary conditions. For this, it is necessary to define the physical model of the problem (Fig. 1) where there is a surface water body with a temperature changing along the day and the seasons, an aquifer of determined thickness where there will be a gradual change of temperature from the bottom to the discharge point and the thermal properties of the aquifer that will be associated to the different characteristics that have different materials. Here we assume that even if flow is coming laterally from the aquifer, in the discharge areas verticalizes favoring the use of 1D temperature-depth profiles.

The mathematical model is formed based on the heat transport equation (simultaneous flow of fluid and heat (Stallman, 1963) plus the new boundary conditions. Initial temperature is also required for the numerical solution.

$$k_m\left(\frac{\partial^2 T}{\partial z^2}\right)-\rho_{e,w}c_{e,w}\left(v_{z,o}\frac{\partial T}{\partial z}\right)-\rho_e c_e\frac{\partial T}{\partial t}=0 \tag{1}$$

$$T_{z=0}=T_{av} \tag{2a}$$

$$T_{(z=0,t)}=T_{av}+\Delta T_{z=0}sin\left(\frac{2\pi}{\tau_o}t\right) \tag{2b}$$

$$T_{z=H}=T_o \tag{3}$$

$$T_{(z,t=0)}=T_{ini} \tag{4}$$

Eq. (1) represents the local balance of heat fluxes: diffusion $\left(k_m\left(\frac{\partial^2 T}{\partial z^2}\right)\right)$, advection $\left(\rho_{e,w}c_{e,w}\left(v_{z,o}\frac{\partial T}{\partial z}\right)\right)$ and storage $\left(\rho_e c_e\frac{\partial T}{\partial t}\right)$, where k_m is the thermal conductivity of the soil-fluid matrix, T is the temperature at any point of the aquifer, z is the vertical coordinate, $\rho_{e,w}$ is the density of water, $c_{e,w}$ is the volumetric heat capacity of water, $v_{z,o}$ is the vertical water flow velocity, ρ_e is the wet bulk density of the rock-fluid matrix, c_e is the volumetric heat capacity of the rock-fluid matrix and t is time.

Boundary conditions for temperature were applied both at the surface and at the bottom. Surface temperature can be considered as constant (Eq. (2a) or seasonally dependent on time (Eq. (2b)) while the bottom of the aquifer is under constant temperature (T_o). T_{ini} is the temperature initial condition (4).

From the mathematical model the relevant parameters and unknowns, such as characteristic lengths and times, are selected. All of them will be part of the lumped parameters (or dimensionless groups) after the non-dimensionalization process. In addition, the normalization of the variables limits their range of values to the interval [0, 1].

Once the dimensionless variables are defined, they are introduced in the governing equation, thus obtaining the dimensionless governing equation, from which the final dimensionless groups can be deduced. To do this, simple mathematical operations are performed with the dimensional coefficients of the equations.

The dimensionless temperature and the dimensionless z position for the case of working with mean temperatures are: $z^{'}=\frac{z}{H}$ and $T^{'}=\frac{T-T_{av}}{T_o-T_{av}}$. Therefore, the appropriate references that have been taken are H for the dimensionless position and temperatures at the ground surface (T_{av}) and at the bottom of the aquifer (T_o) for the dimensionless temperature. Dimensionless time has been defined in the form $t^{'}=\frac{t}{\tau^*}$, where τ^* is the time required to reach steady state conditions. The criterion for choosing τ^* is that temperature at $y=0.9\,H$ (a position far enough from the soil surface) reaches 95 % of its range of variation.

If instead of recording mean temperatures in the aquifer, continuous temperature data are taken at different depths in such a way that the value of the amplitude of the thermal wave can be known, the dimensionless variables are: $\frac{z}{l_{z,o}{}^*}$, $t^{'}=\frac{t}{\tau_o}$ and $T^{'}=\frac{\Delta T}{\Delta T_{z=0}}$, where $l_{z,o}{}^*$ is the depth at which the wave amplitude is negligible (for example, 5 %) compared to the amplitude at the ground surface, τ_o is the period of the sinusoidal wave (daily or seasonally), and $\Delta T_{z=0}$ is the amplitude at the ground surface (see Fig. 1).

Based on the temperature distribution, we have differentiated thermally between shallow and deep aquifers. In a thermally deep aquifer, the total depth H is greater than the characteristic length ($l_{z,o}{}^*$). Therefore, there will be a stretch of aquifer in which the amplitude of the harmonic wave will be negligible. This stretch starts at $z=l_{z,o}{}^*$ and ends at $z=H$. In contrast, in a thermally shallow aquifer, the total depth H is less than the characteristic length ($l_{z,o}{}^*$) as long as the temperature at the bottom of the aquifer is a constant temperature boundary condition. Therefore, since at any point in the aquifer the wave amplitude is not negligible, the dimensionless z position is $z^{'}=\frac{z}{H}$. It is important to highlight that in this work we only differentiate between thermally shallow and thermally deep aquifers if we work with temperature amplitudes measured at different depths instead of with mean temperatures. The advantage is that, for both daily and seasonal periods, the

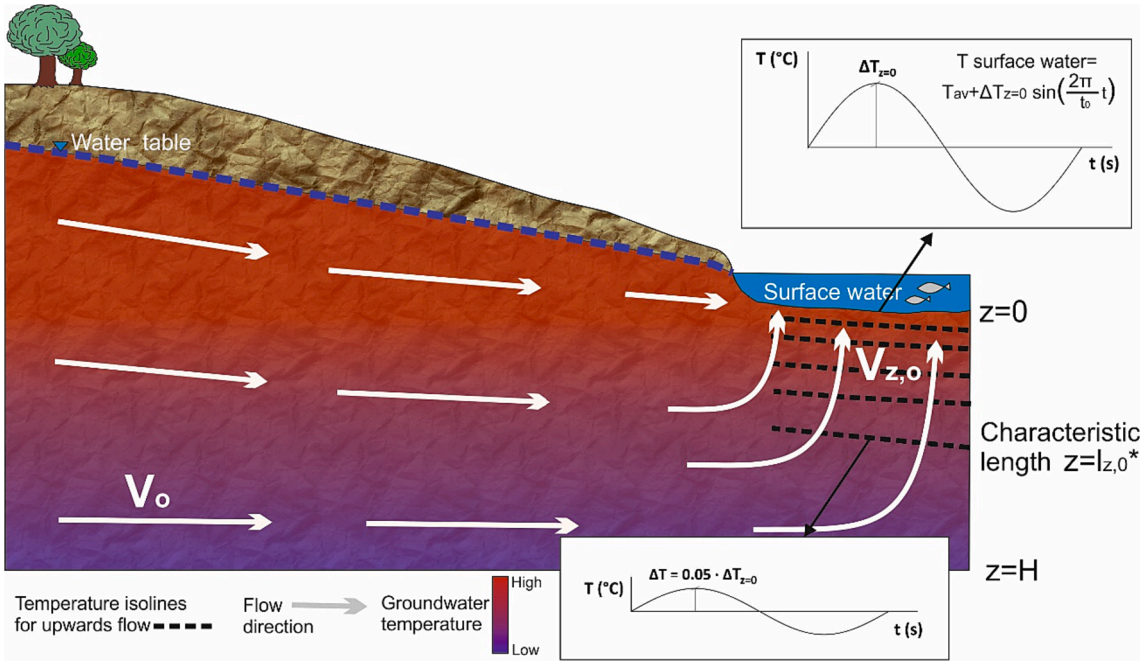

Fig. 1. Physical scheme of the problem.

number of temperature gauges required is less working with amplitudes than with mean temperature profiles.

Once the physical–mathematical model and the dimensionless groups are defined, the last step is the application of the pi theorem: the dimensionless expressions of the unknowns written in their dimensionless form are functions of the dimensionless groups without unknowns (Buckingham, 1914) and, eventually, of the dimensionless position within the domain and dimensionless time (if the problem is transient). In this way, the curves of universal dependencies (solutions) are obtained from numerical simulations carried out from a network (numerical) model using the software Pspice (1994). The main advantage of creating a network model is that we can easily manipulate the mathematical model, simulations are much faster than those of commercial programs and it is easier to work with the results of the simulations. The network model has been created according to the network simulation method (Horno, 2002), a tool applied in engineering coupled problems of similar complexity (Meca et al., 2007; Alhama et al., 2012; Cánovas et al., 2015).

3. Results

The steps to apply the non-dimensionalization process that leads to the dimensionless groups and solutions are included in detail in Appendix A. The set of new solutions for different boundary conditions, both for constant and sinusoidal temperature changes at the aquifer surface, have several applied purposes. Solutions A, B and C are related to a constant temperature boundary condition at the surface, D and E to the harmonic temperature condition and null water flow and, finally, F, G and H to harmonic temperature condition and non-zero water flow (Table 1).

3.1. Constant temperature boundary condition

The graphical solutions for this scenario (Figs. 2 and 3) included curves deduced, point to point, by a large number of numerical simulations. During the transient period, the equation that collects the characteristic time dependence with the monomial $\frac{\alpha}{v_{z,o}H}\left(\frac{\rho_e c_e}{\rho_{e,w}c_{e,w}}\right)$ (Fig. 2) is the same for upward and downward flows. High values of α versus

Table 1
Universal solutions summary.

Universal solutions		Figure
Scenario I Constant temperature boundary condition	$\tau^* = \frac{H^2}{\alpha}\Psi\left\{\frac{\alpha}{v_{z,o}H}\left(\frac{\rho_e c_e}{\rho_{e,w}c_{e,w}}\right)\right\}$	Universal solution B, eq. (A.9, Appendix A)
		Fig. 2
	$T'(z,t) = \frac{T(z)-T_{av}}{T_o-T_{av}} = \Psi\left\{\frac{z}{H}, \frac{t}{\tau^*}\right\}$	Universal solution C, eq. (A.10), Appendix A))
		Fig. 3
Scenario II Harmonic boundary condition with $v_{z,o=0}$	Deep aquifers ($H > l_{z,o}^*$): $(\Delta T')_z = \frac{(\Delta T)_z}{(\Delta T)_{z=0}} = \Psi\left(\frac{z}{l_{z,o}^*}\right)$	Universal solution D, eq. (A.14), Appendix A))
		Fig. 4
	Shallow aquifers ($H < l_{z,o}^*$): $(\Delta T')_z = \frac{(\Delta T)_z}{(\Delta T)_{z=0}} = \Psi\left(\frac{H^2}{\alpha\tau_o}, \frac{z}{H}\right)$	Universal solution E, eq. (A.15), Appendix A))
		Fig. 5
Scenario III Harmonic boundary condition with $v_{z,o} \neq 0$	deep aquifers ($H > l_{z,o}^*$) $l_{z,o}^* = \sqrt{\alpha\tau_o}\Psi\left\{\frac{\alpha}{\tau_o {v_{z,o}}^2}\left(\frac{\rho_e c_e}{\rho_{e,w}c_{e,w}}\right)^2\right\}$	Universal solution F, eq. (A.20, Appendix A))
		Fig. 6
	deep aquifers ($H > l_{z,o}^*$) $\frac{(\Delta T)_z}{(\Delta T)_{z=0}} = \Psi\left(\frac{z}{l_{z,o}^*}\right)$	Universal solution G, eq. (A.22), Appendix A))
		Fig. 7
	shallow aquifers ($H < l_{z,o}^*$) $\frac{(\Delta T)_z}{(\Delta T)_{z=0}} = \Psi\left(\frac{z}{H}, \frac{H^2}{\alpha\tau_o}, \frac{\alpha}{\tau_o {v_{z,o}}^2}\left(\frac{\rho_e c_e}{\rho_{e,w}c_{e,w}}\right)^2\right)$	Universal solution H, eq. (A.23), Appendix A))
		Fig. 8

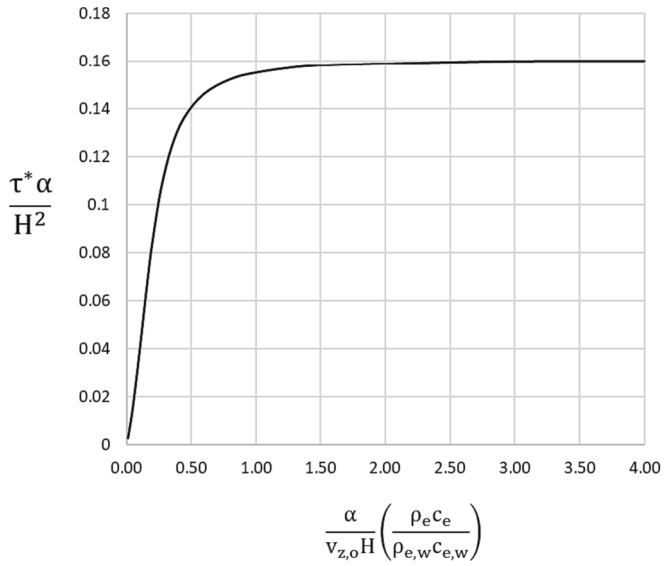

Fig. 2. Constant temperature at the soil surface condition, downward and upward flows. Universal solution B.

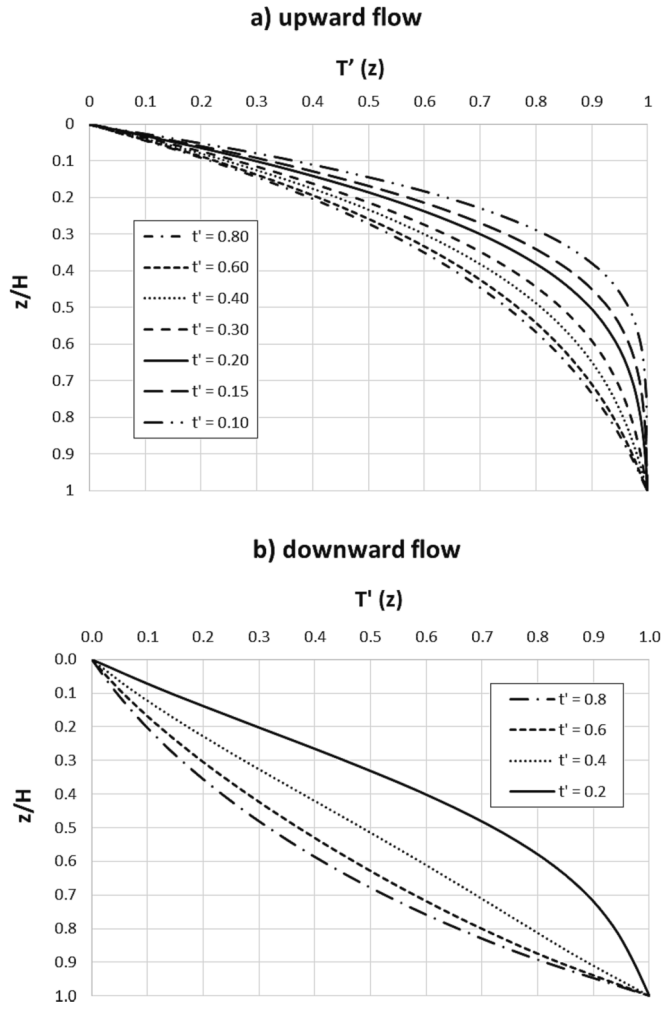

Fig. 3. Constant temperature at the soil surface condition, Universal solution C. a) upward and b) downward flows.

$v_{z,o}H$ do not alter the dimensionless characteristic time $\frac{\alpha\tau^*}{H^2}$, so $\tau^* \frac{H^2}{\alpha}$.

For the dimensionless temperature during the transient period, $T'(z,t) = \frac{T(z)-T_{av}}{T_o-T_{av}} = \Psi\left\{\frac{z}{H}, \frac{t}{\tau^*}\right\}$, there are differences in the curves when flow is upwards or downwards so two graphical sets of curves are needed (Fig. 3). Also the changes associated with $t^{Â}$ are not gradual, and the curves present an uneven distribution with increases of 0.2 for $t^{Â}$.

3.2. Harmonic boundary condition

For the static condition cases (zero water flow), in thermal deep aquifers, the amplitude of the thermal oscillation (Fig. 4) only depends on the relative position $\frac{z}{l_{z,o}}$ (solution D). In thermal shallow aquifers, however, H is a relevant magnitude. The curves converge to the condition of constant temperature (without oscillation) imposed on the bottom, but they have a more constant slope as H decreases until they become a straight line inferred from solution E (Fig. 5).

Solution F for both upward and downward flow is shown in Fig. 6. On the other hand, solution G (Fig. 7) represents the dimensionless amplitude $\frac{(\Delta T)_z}{\Delta T_{z=0}}$ versus relative position referred to characteristic length for scenarios in which there is vertical flow.

When diffusion is greater than advection and groundwater flow is downward, the graphs of dimensionless temperature as a function of z/H (Fig. 8(a) and 8 (b)) are less curved and more sensitive to the parameter $\frac{H^2}{\alpha\tau_o}$ in solution H. Something similar happens for upward flows, Fig. 8 (c) and 8 (d), but in this case the graphs are more sensitive to $\frac{H^2}{\alpha\tau_o}$ when advection is greater than diffusion. Taking the values 0.65 and 0.75 for the ratio $\frac{\rho_e c_e}{\rho_{e,w} c_{e,w}}$, which approximate to real values, and 0.1 and 10 for $\frac{\alpha}{\tau_o v_{z,o}{}^2}$ due to the wide range of $v_{z,o}$, the lumped parameter $\frac{\alpha}{\tau_o v_{z,o}{}^2}\left(\frac{\rho_e c_e}{\rho_{e,w} c_{e,w}}\right)^2$ has the following values: $4.225{\cdot}10^{-2}$ for downward flow a), 4.225 for downward flow b), $5.625{\cdot}10^{-2}$ for upward flow c) and 5.625 for upward flow d).

4. Velocity and parameter estimations

This section first describes the inverse problem approaches that are applicable to Scenarios I, II and III in Table 1. Such approaches are illustrated by their corresponding flow diagrams that explain the successive steps required for the estimations. Second, four applications to real aquifers with field data are presented, one application for each of Scenarios I and II and two applications, one with field data and one with laboratory data, for Scenario III.

4.1. Inverse problem approach

For the case of constant temperature at the ground surface (Scenario I of Table 1), the resulting dependence (see Appendix A, Eq. (A.4) has been tested against the solution of Bredehoeft and Papadopulos (1965) obtaining the same result, verifying that the method proposed address correctly the transport of heat in saturated media. Additionally, it has been generated graphically a set of typed-curves that allows to use it in transient conditions, Figs. 2 and 3.

The steps of this estimation approach are shown in the block diagram in Fig. 9. To estimate the groundwater velocity under these conditions, the depth of the aquifer, its thermal properties as well as boundary conditions are needed, also two vertical temperature profiles at two different real times t_1 and t_2 must be recorded. These two real times are associated with dimensionless times, t_1' and t_2', obtained graphically from Fig. 3.

Each dimensionless time allows to know what percentage of the transient period has been reached. So, for example, a dimensionless time of 0.2 means that 20 % of the time necessary to reach steady state

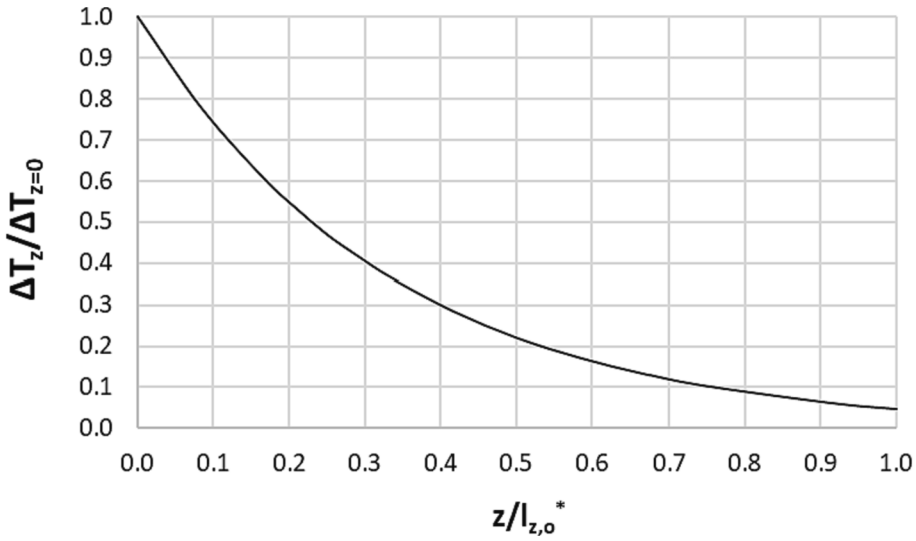

Fig. 4. Harmonic temperature condition at the soil surface and$v_{z,o} = 0$. Universal solution D.

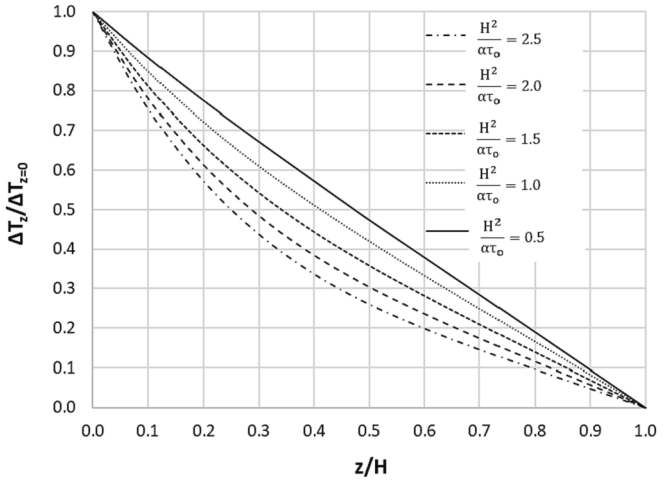

Fig. 5. Harmonic temperature condition at the ground surface and$v_{z,o} = 0$. Universal solution E.

conditions has passed (or, what is the same, 20 % of the characteristic time τ^*). Knowing the time interval between t_1 and t_2 $(t_2 - t_1)$ and the dimensionless times t_1' and t_2', the characteristic time is calculated using the following expression:

$$\tau^* = \frac{t_2 - t_1}{(t_2' - t_1')} \tag{5}$$

Once the value of the characteristic time (τ^*) is known, Fig. 3 provides the balance between advective and diffusive flows, $\frac{\alpha}{v_{z,o}H}\left(\frac{\rho_e c_e}{\rho_{e,w} c_{e,w}}\right)$, an expression from which $v_{z,o}$ is deduced. In order to use this method, it is necessary to know or assume an order of magnitude of the thermal properties of the aquifer and its depth (H).

The scenarios II and III refer to cases in which the temperature at the surface varies continuously based on diurnal and seasonal conditions. This is often a challenge that is solved by assuming measurements of the amplitude of the thermal oscillations. To do this, a characteristic length can be identified as the depth at which the amplitude of the thermal wave is negligible compared to the amplitude of the temperature oscillation at the ground surface. We have named it $l_{z,o}^*$. It also allows to divide the aquifers from the thermal point of view in two types. Firstly,

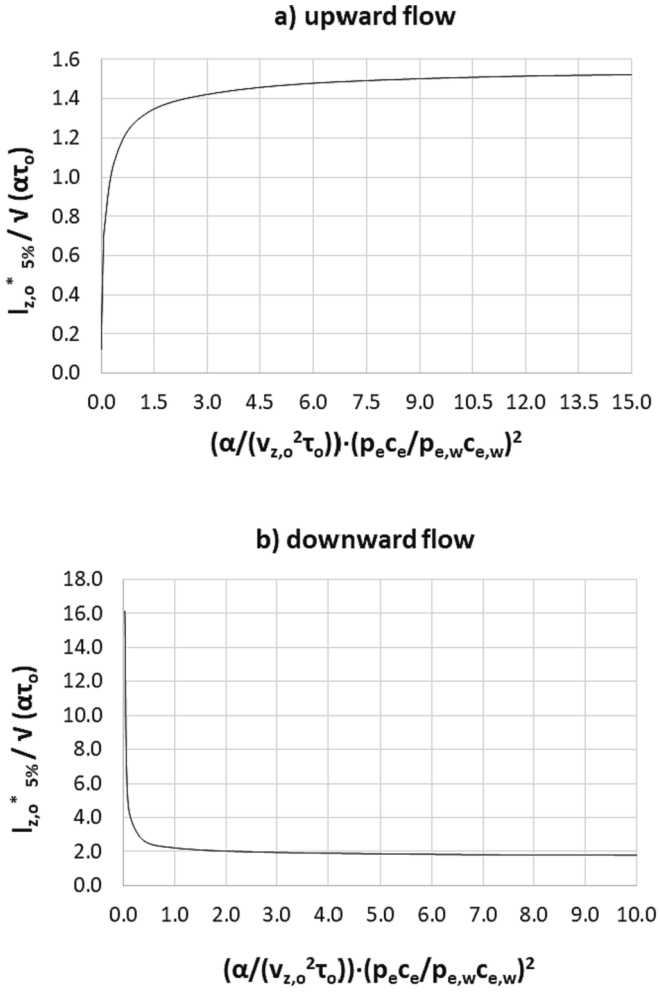

Fig. 6. Harmonic temperature condition at the soil surface and$v_{z,o} \neq 0$. Universal solution F. a) upward and b) downward flows.

the thermally shallow aquifers, which are those in which the amplitude of the thermal wave is not negligible throughout its whole thickness. In these aquifers there is no characteristic length and their depth H becomes a relevant parameter for the solution of the problem. Secondly,

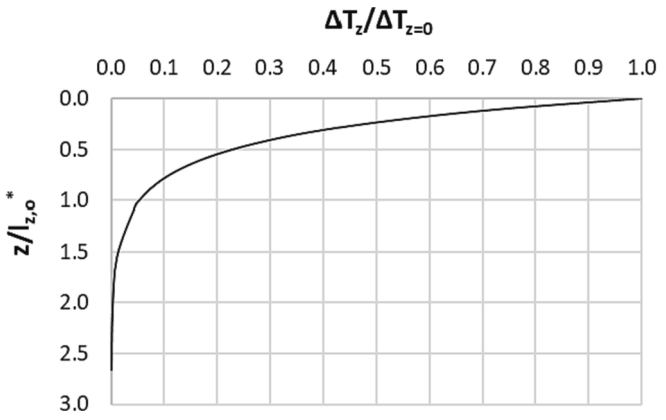

Fig. 7. Harmonic temperature at the soil surface and$v_{z,o} \neq 0$. Universal solution G.

the most frequent scenario we will call thermally deep aquifers. In this, the total depth H is an irrelevant parameter and instead a characteristic length can be introduced to define the subregion in which temperature oscillations are appreciable.

Fig. 10 shows the flow diagram for the case of zero groundwater velocity, $v_{z,o} = 0$, Scenario II. From the input data, $(\Delta T)_{z=0}$, $(\Delta T)_{z_1}$, $(\Delta T)_{z_2}$, z_1, z_2 and H, the dimensionless temperature deviations, $\frac{(\Delta T)_{z_1}}{(\Delta T)_{z=0}}$ and $\frac{(\Delta T)_2}{(\Delta T)_{z=0}}$ are obtained. From them, Fig. 4 allows to read two characteristic lengths, $l_{z,o}{}^*{}_1$ and $l_{z,o}{}^*{}_2$. If $l_{z,o}{}^*{}_1 \approx l_{z,o}{}^*{}_2$, this is the characteristic length of the problem while the termal diffusivity is deduced from the expression (A.13),$l_{z,o}{}^* = 1.668\sqrt{\alpha\tau_o}$.

If $l_{z,o}{}^*{}_1 \neq l_{z,o}{}^*{}_2$, Fig. 5 allows to read the value of the lumped parameter $\frac{H^2}{\alpha\tau_o}$ of the curve most close to the field temperature profile and to estimate the thermal diffusivity from it.

Finally, the approach that estimates the groundwater velocity from thermal wave deviations at different depths is shown in Fig. 11. As in scenario II, from the input data $(\Delta T)_{z=0}$, $(\Delta T)_{z_1}$, $(\Delta T)_{z_2}$, z_1 and z_2, the ratios $\frac{(\Delta T)_{z_1}}{(\Delta T)_{z=0}}$ and $\frac{(\Delta T)_2}{(\Delta T)_{z=0}}$ allow to read the values of $\frac{z_1}{l_{z,o}}$ and $\frac{z_2}{l_{z,o}}$ in Fig. 7. If these two values provides the same $l_{z,o}{}^*$, we can affirm that this is a thermally deep aquifer. Entering in Fig. 6 a) or 6b), depending on upward or downward flow, with $\frac{l_{z,o}{}^*}{\sqrt{\alpha\tau_o}}$, the group $\frac{\alpha}{\tau_o v_{z,o}{}^2}\left(\frac{\rho_e c_e}{\rho_{e,w} c_{e,w}}\right)^2$ is read and

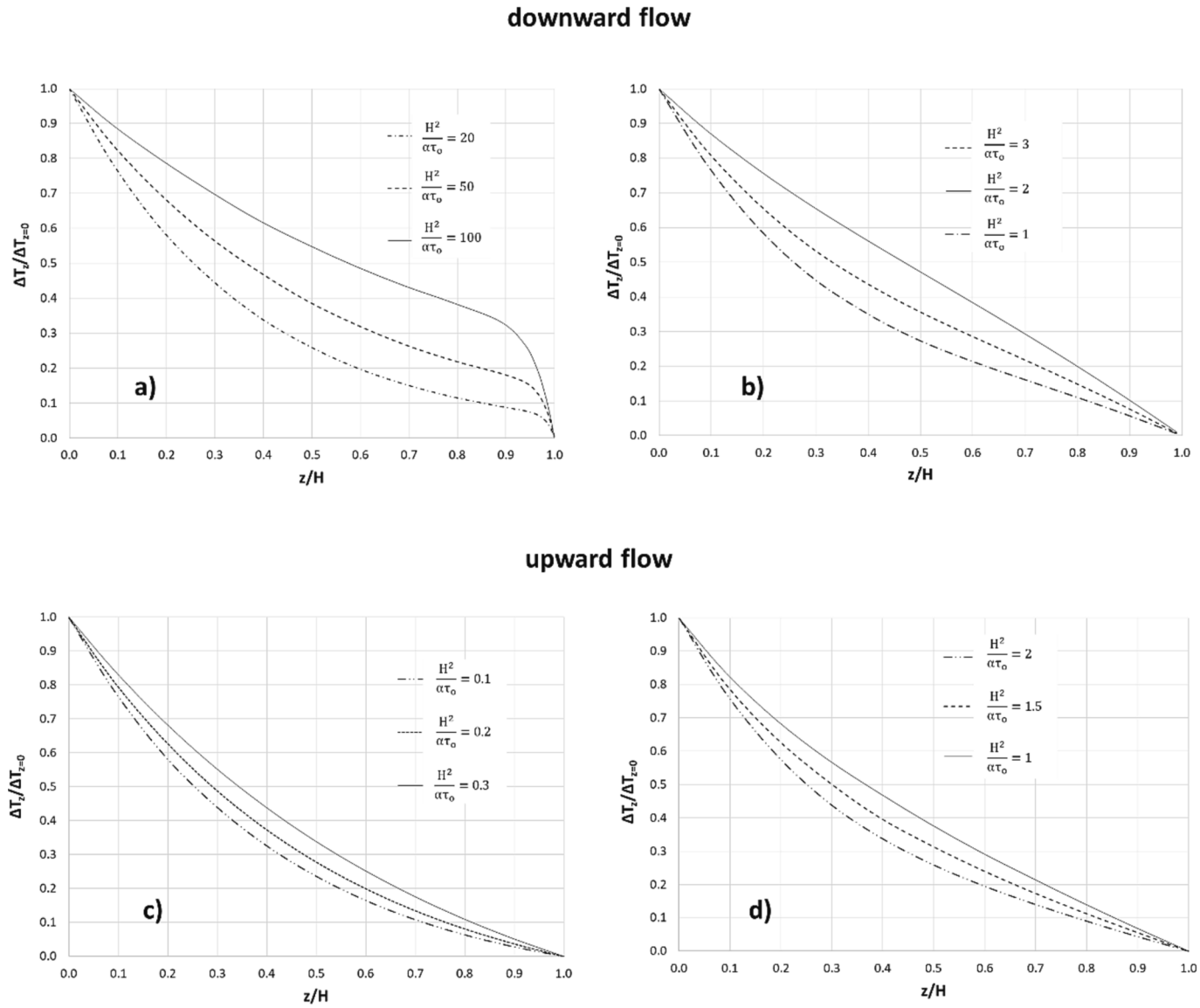

Fig. 8. Harmonic temperature at the soil surface and$v_{z,o} \neq 0$. Universal set of solutions. H.

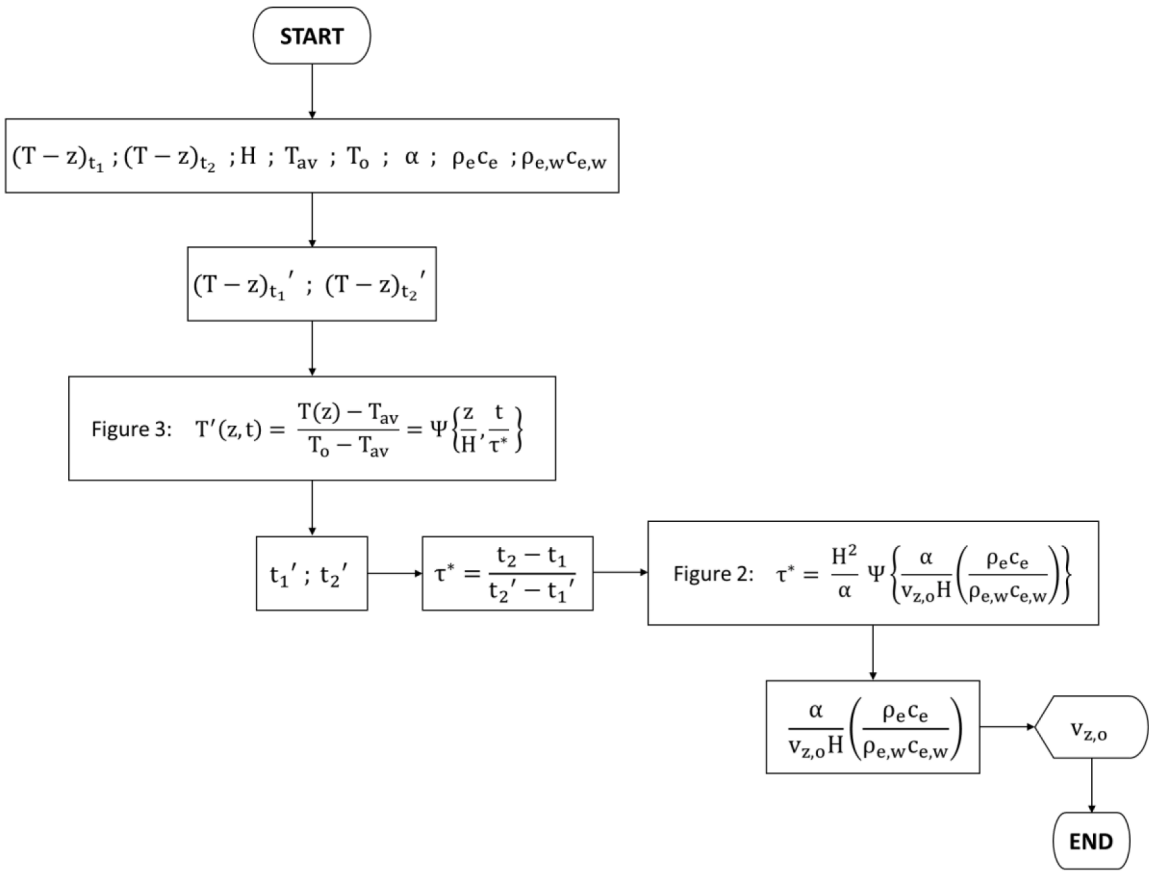

Fig. 9. Flow diagram for the solution of the inverse problem, Scenario I.

from this the velocity $v_{z,o}$ estimated. In the case of thermal shallow aquifers with H a known data, entering with the pairs $\left(\frac{(\Delta T)_{z_1}}{(\Delta T)_{z=0}}, \frac{z_1}{H_1}\right)$ and $\left(\frac{(\Delta T)_{z_2}}{(\Delta T)_{z=0}}, \frac{z_2}{H_1}\right)$, and the parameter of the curve $\frac{H^2}{\alpha\tau_o}$ within the same abacus, the curve that best fits to the pairs allow to obtain the parameter of the abacus $\frac{\alpha}{\tau_o v_{z,o}{}^2}\left(\frac{\rho_e c_e}{\rho_{e,w} c_{e,w}}\right)^2$ from which the velocity is estimated.

4.2. Applications to real scenarios

To verify the dependencies of Table 1, four applications to real scenarios are presented. For scenarios I and II, the field data come from the historical series of groundwater temperature in the piezometric network of 'Agua Amarga' salt marsh, in Alicante, SE of Spain. During the period 2008–2023, the coastal aquifer was submitted to an aquifer recharge program with seawater to restore piezometric depletion and to promote vegetation on the surface (Alhama et al., 2022). As regards scenario III, the input data came from the experimental measurements obtained by Hatch et al. (2006) in Pajaro River (California, USA) and by Lautz (2012) in two laboratory experiments denominated 'Step Change experiment' and 'Gradual Change experiment'.

In relation to the errors associated with the reading of data in the universal curves of Section 3, it must be said that these are refined readings, with negligible errors, since such curves have been obtained point by point by means of very precise numerical solutions. Due to their length, these tabulated data are not presented in this work.

4.2.1. Scenario I

For this scenario, the data correspond to temperature-depth profiles for each meter depth at P-8, which were already used to deduce upward flow velocity (between $2{\cdot}10^{-9}$ and $7.5{\cdot}10^{-7}$ m/s) following a standard scheme of inverse problem, Jiménez-Valera et al. (2023). Once the artificial recharge of the aquifer stops (July 19, 2022) and the transient period starts, temperature profiles are taken at times t_1 (September, 16) and t_2 (October, 21), $t_2 - t_1 = 34$ days.

Fig. 12 a) incorporates to the universal transient curves (Fig. 3, $T'(z,t) = \frac{T(z)-T_{av}}{T_o-T_{av}} = \psi\left\{\frac{z}{H}, \frac{t}{\tau^*}\right\}$) the P-8 profiles, measured meter by meter depth. Since these are instantaneous measurements that reflect the sensitive influence of the boundary (ambient) temperature condition, such profiles modify their trajectory appreciably as they approach the surface, and thus move away from the universal profiles unaffected by this condition. To avoid the errors introduced by this effect, the upper part of the profile (the subregion $0<z' < 0.3$, approximately) is removed leaving us with the temperature data at depths below $z' = 0.3$, Fig. 12 b).

The curves that best fit these data correspond to dimensionless times of value $t_1{}' = 0.25$ and $t_2{}' = 0.30$. The expression $\tau^* = \frac{t_2-t_1}{(t_2'-t_1')}$ allows to deduce the value of the characteristic time (approximate duration of the transient), $\tau^* = 58752000$ s or 680 days, to which corresponds a dimensionless time of $\frac{\tau^*\alpha}{H^2} = \frac{58752000 \cdot 3.6 \cdot 10^{-6}}{50^2} = 0.085$. From this data Fig. 2 estimates for the lumped parameter $\frac{\alpha}{v_{z,o}H}\left(\frac{\rho_e c_e}{\rho_{e,w} c_{e,w}}\right)$ a value of 0.20, which, in turn allows to obtain the velocity, $v_{z,o} = 3.25 \cdot 10^{-7}$ m/s. A value slightly below the upper limit deduced by classical inverse problem approaches.

4.2.2. Scenario II

This application estimates the thermal diffusivity of the aquifer, without experimental equipment, from the temperature oscillations at different depths in P-4 piezometer. The analysis of piezometric time series in the surrounding of P-4, drilled in Pliocene- Pliocene-Pleistocene

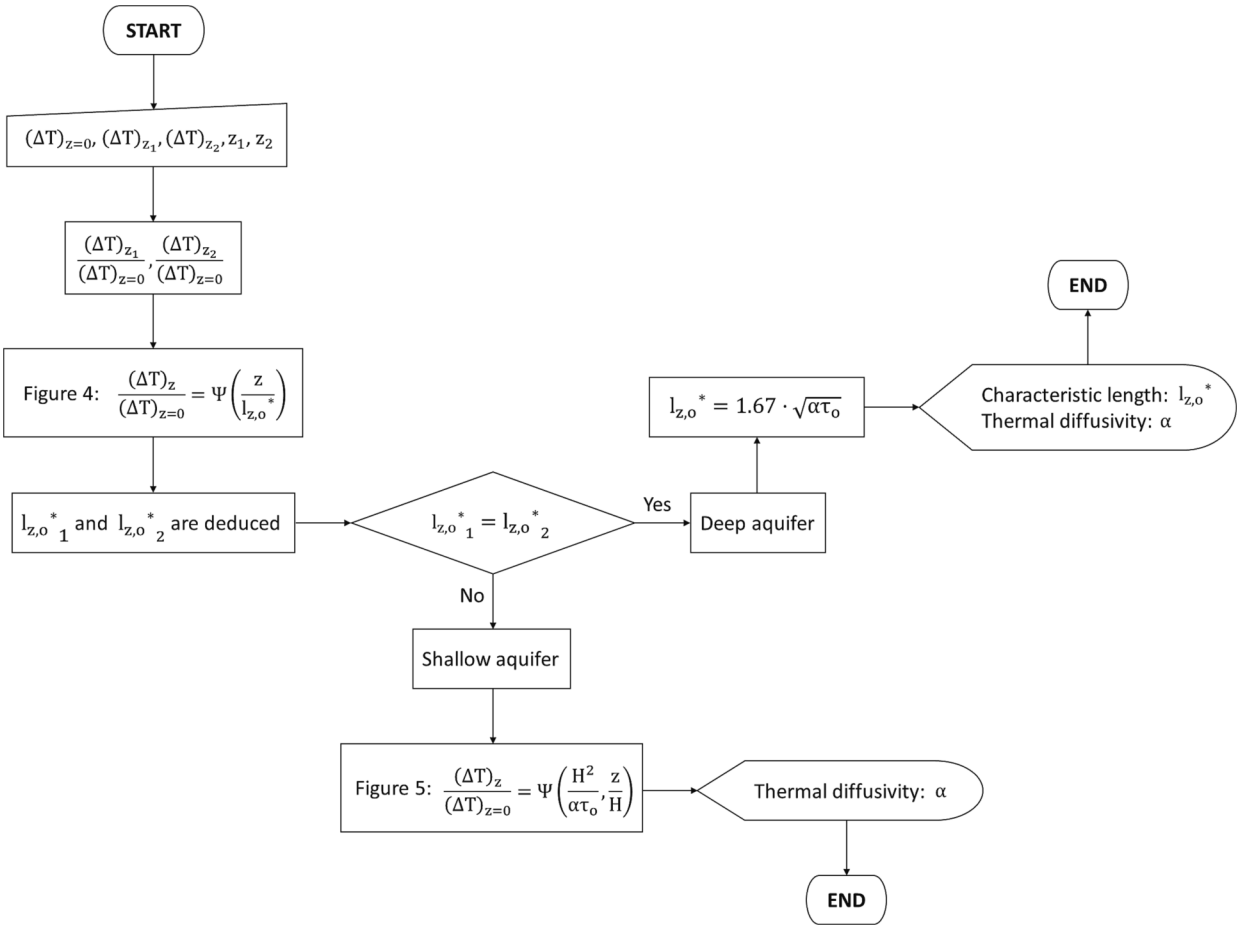

Fig. 10. Flow diagram for the solution of the inverse problem, Scenario II.

continental sand-silt of K (m/d) of the order of 0.008 (Alhama, 2013), has allowed to assess the mean hydraulic gradient in the area around 0.4. These data provides a groundwater flow velocity in this region of value $3.7{\cdot}10^{-8}$ m/s which we will assume negligible for advection heat transport process.

Temperature measurements were taken at the ground surface and at depths of 10 and 13 m between December 2020 and December 2021. The results are shown in Table 2.

Entering Fig. 5 which represents the universal solution $\frac{(\Delta T)_z}{(\Delta T)_{z=0}} = \psi\left(\frac{z}{l_{z,o}^*}\right)$, we obtain the relative positions $\frac{z_1}{l_{z,o}^*{}_1}$ and $\frac{z_2}{l_{z,o}^*{}_2}$ which allow us to verify that the characteristic lengths are identical and thus confirm that this is a deep aquifer. According to Figure, for $\frac{\Delta T_{z=-10}}{\Delta T_{z=0}} = 0.175$ results $\frac{z_1}{l_{z,o}^*{}_1} = 0.56$, while for $\frac{\Delta T_{z=-13}}{\Delta T_{z=0}} = 0.11$ results $\frac{z_2}{l_{z,o}^*{}_2} = 0.73$. These values, $l_{z,o}^*{}_1 = 17.85$ and $l_{z,o}^*{}_2 = 17.8$, very close to each other, confirm that this is a deep aquifer. Finally, from the expression $l_{z,o}^* = 1.668\hat{A}{\cdot}\sqrt{\alpha\tau_o}$, a thermal diffusivity of value $\alpha = 3.6\hat{A}{\cdot}10^{-6}$ m^2/s is estimated, relatively high but within the expected range for this type of aquifers (Lapham, 1989).

4.2.3. Scenario III. Application with field data from Hatch et al. (2006)

Field data for this aquifer are thermal amplitudes at two different depths in the riverbed: $\Delta T_{z_1} = 2.00$ °C, $\Delta T_{z_2} = 1.20$ °C, $z_1 = 0.1$ m and $z_2 = 0.4$ m. These values have been recorded beneath the Pajaro River streambed on the central California coast. Since the oscillation at the streambed surface is an unknown, an iterative approach is needed for estimation. The parameters of the problem are shown in Table 3.

To follow the flow diagram of Fig. 11 we will propose to perform iterations assuming successively increasing or decreasing values of $(\Delta T)_{z=0}$ until, for both depths (z_1 and z_2), the universal curve of Fig. 7 provides values of $\frac{z_1}{l_{z,o}^*{}_1}$ and $\frac{z_2}{l_{z,o}^*{}_2}$ leading to very approximate values of $l_{z,o}^*{}_1$ and $l_{z,o}^*{}_2$. Starting from the initial value $(\Delta T)_{z=0} = 2.5$, Table 3 shows some of the partial results of $l_{z,o}^*{}_1$ and $l_{z,o}^*{}_2$ that clearly converge to a characteristic length for their aquifer of value $l_{z,o}^* \approx 1.7486$ and a temperature oscillation of $\Delta T_{surface}$. ≈ 2.35.

Entering $l_{z,o}^* \approx 1.7486$, $\frac{l_{z,o}^*}{\sqrt{\alpha\tau_o}} = 5.9489$ in Fig. 6 (downstream flow), $\frac{\alpha}{\tau_o v_{z,o}{}^2}\left(\frac{\rho_e c_e}{\rho_{e,w} c_{e,w}}\right)^2 = 0.07574$ is obtained, resulting in an estimated velocity of $1.236{\cdot}10^{-5}$ m/s (1.068 m/d). The velocity quantified by Hatch et al. (2006) using time-series analysis of stream bed thermal records is approximately 1.20 m/d. The difference between the two estimated velocities is about 10 %. Considering that $\Delta T_{surface}$ and $l_{z,o}^*$ have been estimated graphically from the universal curves and that ΔT_{z_1}, ΔT_{z_2} and the value of the Hatch vertical velocity has also been estimated likewise from their graphical solutions, it can be concluded that the comparison is satisfactory. See Table 4.

4.2.4. Scenario III. Application with laboratory data from Lautz (2012)

In the first Lautz laboratory experiment, the flow rate changed instantaneously (step change experiment) in a sand column while, in the second it decreased gradually over an 8-hour interval (gradual change experiment). The scenario parameters are reflected in Table 5:

Using the approach proposed for Scenario III, the inverse problem for estimating $v_{z,o}$ assumes as input data the amplitude of the thermal wave oscillations at different depths. For the first experiment these data, read

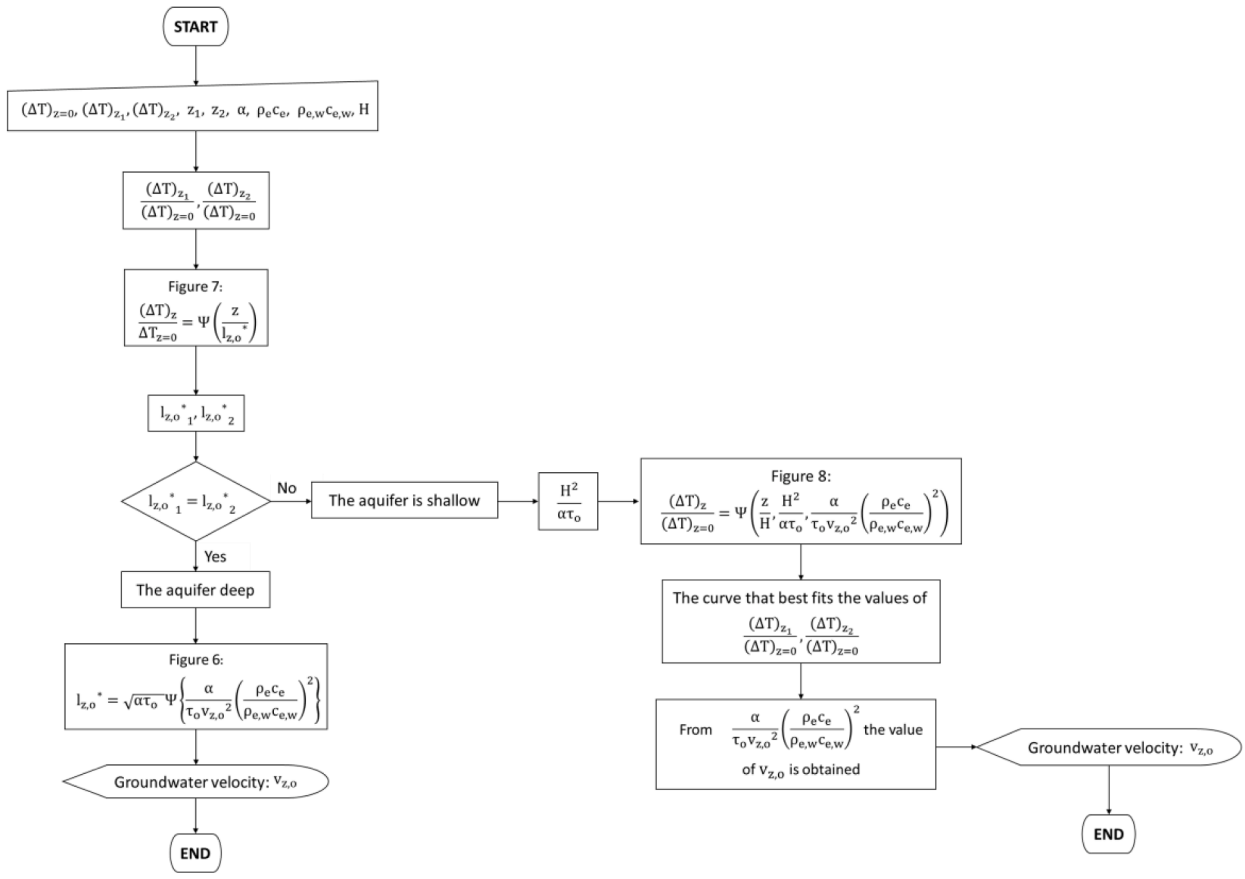

Fig. 11. Flow diagram for the solution of the inverse problem, Scenario III.

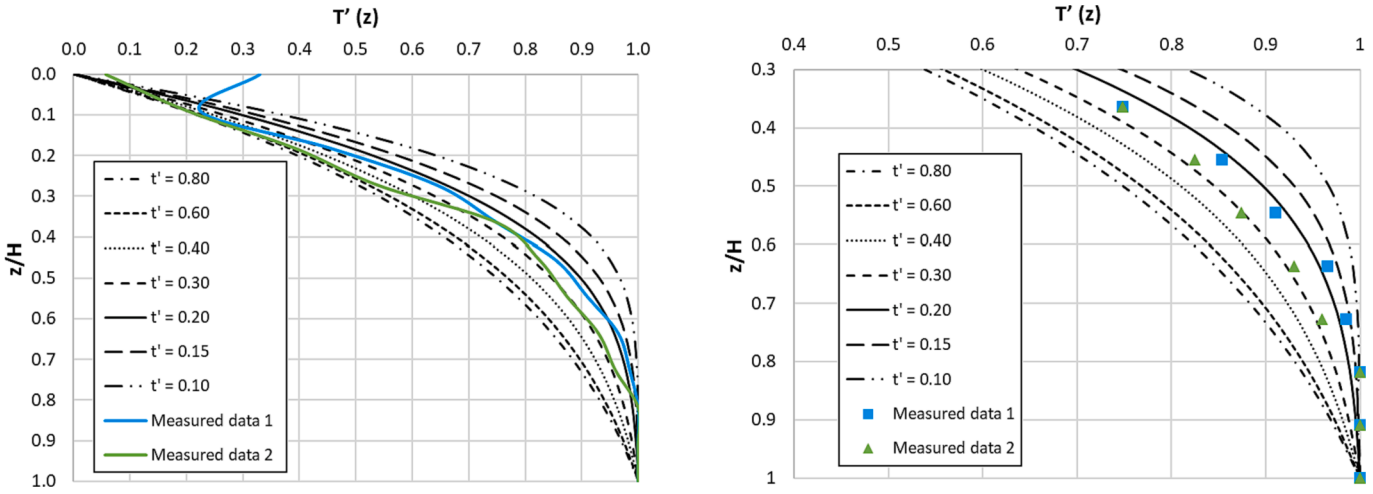

Fig. 12. a) Dimensionless profiles of piezometer P-8 within the abacus of universal profiles. b) Detail of the figure for depths below $z' = 0.3$.

Table 2
Temperature oscillations in P-4.

z(m)	0.00	−10.0	−13.00
ΔT	2.85	0.50	0.30

Table 3
Parameters of scenario in Hatch et al. (2006).

Parameter	Value
λ_o(Js^{-1}m^{-1}°C^{-1})	1.00
$\rho_{e,w}c_{e,w}$(J °C^{-1}m^{-3})	4.18
$\rho_e c_e$(J °C^{-1}m^{-3})	4.18
τ_o (h)	24.00

Table 4
Partial results of characteristic lengths $l_{z,o}{}^*{}_{z_1}$ and $l_{z,o}{}^*{}_{z_2}$ for different values of $\Delta T_{surface}$.

$\Delta T_{surface}$(°C)	$l_{z,o}{}^*{}_{z_1}$ (m)	$l_{z,o}{}^*{}_{z_2}$ (m)	$\lvert l_{z,o}{}^*{}_{z_2}\text{-}l_{z,o}{}^*{}_{z_1}\rvert$ *(m)*
2.335	1.812	1.765	0.047
2.340	1.792	1.760	0.032
2.350	1.748	1.749	0.001
2.360	1.704	1.739	0.035

Table 5
Parameters of Lautz (2012).

Parameter	Value
λ_o(Js^{-1}m^{-1}°C^{-1})	3.4
$\rho_{e,s}c_{e,s}$(J °C^{-1}m^{-3})	3.6
$\rho_{e,w}c_{e,w}$(J °C^{-1}m^{-3})	4.2
$\rho_e c_e$(J °C^{-1}m^{-3})	4.0
τ_o (h)	6.0

Table 6
Partial results of $l_{z,o}{}^*{}_{z_1}$ and $l_{z,o}{}^*{}_{z_2}$ for increasing values of $\Delta T_{surface}$.

$\Delta T_{surface}$(°C)	$l_{z,o}{}^*{}_{z_1}$ (m)	$l_{z,o}{}^*{}_{z_2}$ (m)	$\lvert l_{z,o}{}^*{}_{z_2}\text{-}l_{z,o}{}^*{}_{z_1}\rvert$ (m)
2.15	1.136	0.935	0.201
2.20	0.977	0.873	0.104
2.25	0.848	0.820	0.028
2.27	0.807	0.800	0.007

from cycles 15–19 of a Lautz plot, are: $\Delta T_{z_1} = 1.905$ °C, $\Delta T_{z_2} = 1.570$ °C, $z_1 = 0.05$ m and $z_2 = 0.1$ m. As in subsection 4.2.3, Table 6 shows the partial results of $l_{z,o}{}^*{}_1$ and $l_{z,o}{}^*{}_2$, obtained with Fig. 7. The first value of $\Delta T_{surface}$ is 2 °C. The difference $l_{z,o}{}^*{}_{z_2}$-$l_{z,o}{}^*{}_{z_1}$ becomes negligible for $\Delta T_{surface} = 2.27$ °C, providing$l_{z,o}{}^*{}_{z_2} = 0.8$ m and$l_{z,o}{}^*{}_{z_1} = 0.807$ m. The dimensionless characteristic length is then $\frac{l_{z,o}{}^*}{\sqrt{\alpha\tau_o}} = 5.904$. Entering this value in Fig. 6 (downward flow) $\frac{\alpha}{\tau_o v_{z,o}{}^2}\left(\frac{\rho_e c_e}{\rho_{e,w}c_{e,w}}\right)^2 = 0.0746$ and$v_{z,o} = 2.187{\cdot}10^{-5}$ m/s, a value very close to that provided by Lautz, $v_{z,o,Lautz} = 2{\cdot}10^{-5}$ m/s using the numerical software VFLUX (Gordon et. al, 2012).

For the gradual change experiment, the input data read from cycles 4–5 are: $\Delta T_{z_1} = 2$ °C, $\Delta T_{z_2} = 1.862$ °C, $z_1 = 0.05$ m an $dz_2 = 0.1$ m. The first value used for $\Delta T_{surface}$ is 2.5 °C. The partial results, shown in Table 7, lead to the solution $\Delta T_{surface} = 2.135$ °C, $l_{z,o}{}^*{}_{z_2} = 2.033$ m and$l_{z,o}{}^*{}_{z_1} = 2.041$ m. Entering Fig. 6 with $\frac{l_{z,o}{}^*}{\sqrt{\alpha\tau_o}} = 15$, $\frac{\alpha}{\tau_o v_{z,o}{}^2}\left(\frac{\rho_e c_e}{\rho_{e,w}c_{e,w}}\right)^2 = 0.0325$ results and the estimated velocity is$v_{z,o} = 3.31{\cdot}10^{-5}$ m/s, again, a value close to the estimated velocity by Lautz with VFLUX, $v_{z,o} = 3{\cdot}10^{-5}$ m/s.

5. Conclusions

A new set of solutions (type curves) is proposed to estimate, using heat as a tracer, the vertical groundwater flow and other thermal parameters in aquifers with different boundary conditions. The applied methodology is based on the non-dimensionalization of the governing equation and boundary conditions, whose result, after certain mathematical manipulations, provides the lumped parameter or dimensionless groups that govern the solution of these problems. These groups arise from the balance between the terms of the dimensionless governing equations. The independent variables of the problem, position and time, are defined dimensionless using well-chosen references. For the position, the depth from which the oscillations have a negligible amplitude compared to the amplitude of the wave at the ground surface is adopted as a reference, while for the time, the duration of the transient period is taken as a reference. The Pi theorem establishes the functional dependencies between deduced lumped parameters and a large number of numerical simulations make it possible to represent such dependencies by means of universal type curves or abacuses.

Table 7
Partial results of $l_{z,o}{}^*{}_{z_1}$ and $l_{z,o}{}^*{}_{z_2}$ for decreasing values of $\Delta T_{surface}$.

$\Delta T_{surface}$(°C)	$l_{z,o}{}^*{}_{z_1}$ (m)	$l_{z,o}{}^*{}_{z_2}$ (m)	$\lvert l_{z,o}{}^*{}_{z_2}\text{-}l_{z,o}{}^*{}_{z_1}\rvert$ (m)
2.200	1.429	1.695	0.266
2.150	1.852	1.946	0.094
2.140	1.969	2.000	0.031
2.135	2.041	2.033	0.008

The scenarios studied cover most of the real cases of aquifers with vertical groundwater flow (downward and upward), including the use as input data of the mean temperature or the amplitude of the wave oscillation, in addition to the cases of transient temperature profiles. These scenarios are: i) Step temperature change at the surface (a transient case) for groundwater velocity estimation, ii) Harmonic temperature oscillation at the surface without groundwater flow for estimation of thermal diffusivity of the soil–water matrix, and iii) Harmonic temperature oscillation at the surface for estimation of vertical groundwater velocity. The methodology for these estimations is based on specific inverse problem approaches using the universal curves for each scenario and simple mathematical expressions derived from non-dimensionalization. The proposed schemes have been illustrated by flow diagrams to facilitate their use by hydrogeologists.

For the case of constant soil surface temperature scenario, the derived stationary solutions agree with those of Bredehoeft and Papadopulos (1965). For the transient case (Scenario I of Table I), the universal curves obtained represent the solution of the dimensionless characteristic time and the dimensionless transient temperature profiles, graphs that allow the estimation of the vertical flow of groundwater.

Sinusoidal temperature changes at the surface require establishing a distinction, from a thermal point of view, between deep and shallow thermal aquifers, which is achieved by introducing a characteristic length whose expression is deduced for Scenarios II and III.

For scenario II, universal curves are presented that show the dimensionless temperature amplitude for both deep and shallow aquifers. Such curves allow the estimation of the thermal diffusivity of the water-soil matrix. Finally, for scenario III, universal curves of the dimensionless characteristic length and thermal amplitude for deep aquifers and a set of universal abacuses of the dimensionless amplitude for shallow aquifers are deduced. These curves allow us to estimate the groundwater velocity in this last scenario.

Three applications of real aquifers are presented, and a fourth with laboratory data, which cover all the scenarios studied in this work. In all of them, the value of the parameters estimated following the proposed approaches is successfully compared with analytical results from other authors or those derived from indirect field measurements.

CRediT authorship contribution statement

José Antonio Jiménez-Valera: Conceptualization, Data curation, Formal analysis, Funding acquisition, Investigation, Methodology, Resources, Software, Validation, Visualization, Writing – original draft, Writing – review & editing. **Iván Alhama:** Data curation, Formal analysis, Resources, Supervision, Writing – review & editing, Methodology, Validation. **Carlos Duque:** Data curation, Formal analysis, Investigation, Methodology, Resources, Supervision, Validation, Visualization, Writing – review & editing, Writing – original draft, Conceptualization, Funding acquisition.

Declaration of competing interest

The authors declare the following financial interests/personal relationships which may be considered as potential competing interests: Jose Antonio Jimenez Valera reports financial support was provided by Fundación Séneca. Carlos Duque reports financial support was provided by Programa María Zambrano Sénior.

Data availability

References are added

Acknowledgments

This work was supported by "Fundación Séneca" (scholarship awarded to José Antonio Jiménez Valera), "21271/FPI/19. Fundación Séneca. *Región de Murcia (Spain)*" and the Next-Generation EU funding: Programa María Zambrano Sénior (REF: MZSA03).

Appendix A. . Non-dimensionalization and universal dependences

Constant temperature at the ground surface.

The steady-state solution reduces Eq. (1) to

$$k_m\left(\frac{\partial^2 T}{\partial z^2}\right) - c_{e,w}\rho_{e,w}\left(v_{z,o}\frac{\partial T}{\partial z}\right) = 0 \tag{A.1}$$

The dimensionless normalized variables z' and T' are defined in the form

$$z' = \frac{z}{H}; T' = \frac{T - T_{av}}{T_o - T_{av}}$$

whose values are confined to the interval $[0, 1]$. Introducing these variables in Eq. (A.1)

$$\frac{k_m(T_o - T_{av})}{H^2}\frac{\partial^2 T'}{\partial z'^2} - \frac{v_{z,o}c_{e,w}\rho_{e,w}(T_o - T_{av})}{H}\frac{\partial T'}{\partial z'} = 0 \tag{A.2}$$

Re-grouping coefficients, simplifying and introducing $\alpha = \frac{k_m}{c_{e,}\rho_e}$, eq. (A.2) yields

$$\frac{\alpha}{H}\left(\frac{c_e\rho_e}{c_{e,w}\rho_{e,w}}\right)\frac{\partial^2 T'}{\partial z'^2} - v_{z,o}\frac{\partial T'}{\partial z'} = 0 \tag{A.3}$$

Approximating the derivatives of the dimensionless variables to unity thanks to the normalization (Bejan, 2013), and operating, the previous equation provides the dimensional group π_1:

$$\pi_1 = \frac{\alpha_c}{v_{z,o}H} = \frac{\alpha}{v_{z,o}H}\left(\frac{c_e\rho_e}{c_{e,w}\rho_{e,w}}\right)$$

This group is the ratio between the simplified addends of the equation. By applying pi theorem (Buckingham, 1914), the steady state solution of the dimensionless form of T' defined as $T'(z) = \frac{T(z) - T_{av}}{T_o - T_{av}}$ is a function of π_1 as well as of the dimensionless depth $z' = z/H$:

$$T'(z) = \frac{T(z) - T_{av}}{T_o - T_{av}} = \Psi\left\{\frac{\alpha}{v_{z,o}H}\left(\frac{c_e\rho_e}{c_{e,w}\rho_{e,w}}\right), \frac{z}{H}\right\} \text{(Universal solution A)} \tag{A.4}$$

This solution (A.4) is the same as Bredehoeft and Papadopulos (1965), who obtained it by numerically solving the equation.

For the transient solution, τ^* is defined as the time required for steady state temperature profiles to be reached. Defining the dimensionless time in the form $t' = \frac{t}{\tau^*}$ (to be closely normalized to the interval [0,1]), and introducing it in eq. (1), the dimensionless governing equation for the transient period is

$$\frac{\alpha}{H^2}\frac{\partial^2 T'}{\partial z'^2} - \frac{v_{z,o}}{H}\left(\frac{c_{e,w}\rho_{e,w}}{c_e\rho_e}\right)\frac{\partial T'}{\partial z'} = \frac{1}{\tau^*}\frac{\partial T'}{\partial t'} \tag{A.5}$$

Again, approximating the derivatives of the dimensionless variables to unity and operating, the independent dimensionless groups that rule the solution are obtained. These groups are named π_1 (ratio between the first and second addends) and π_{τ^*} (ratio between the second and third addends):

$$\pi_1 = \frac{\alpha}{v_{z,o}H}\left(\frac{c_e\rho_e}{c_{e,w}\rho_{e,w}}\right) \tag{A.6}$$

$$\pi_{\tau^*} = \frac{v_{z,o}}{H}\left(\frac{c_{e,w}\rho_{e,w}}{c_e\rho_e}\right)\tau^* \tag{A.7}$$

By applying pi theorem (Buckingham, 1914], he solution for τ^* is $\pi_{\tau^*} = f(\pi_1)$, or

$$\tau^* = \frac{H}{v_{z,o}}\frac{c_e\rho_e}{c_{e,w}\rho_{e,w}}\Psi\left\{\frac{\alpha}{v_{z,o}H}\left(\frac{c_e\rho_e}{c_{e,w}\rho_{e,w}}\right)\right\} \tag{A.8}$$

Since the quotient $\frac{c_e\rho_e}{c_{e,w}\rho_{e,w}}$ is very close to 1 in most aquifers, $f(\pi_1)$ may be considered as an only function of $\frac{\alpha}{v_{z,o}H}$. Choosing the pair of independent

groups, $\pi_1 = \frac{\alpha}{v_{z,o}H}\left(\frac{c_e\rho_e}{c_{e,w}\rho_{e,w}}\right)$ and $\pi_{\tau^*} = \frac{H^2}{\alpha\tau^*}$, the solution for τ^* can alternatively be expressed in the form.

$\tau^* = \frac{H^2}{\alpha}\Psi\left\{\frac{\alpha}{v_{z,o}H}\left(\frac{c_e\rho_e}{c_{e,w}\rho_{e,w}}\right)\right\}$ (Universal solution B) (A.9).

These last expressions, (A.8) and (A.9), can be particularized by adopting a criterion for the definition of τ^*, for example the time required to reach 95 (or 99) % of the steady state temperature expressed in dimensionless form ($T'(z) = \frac{T(z)-T_{av}}{T_o-T_{av}}$). The transient temperature at each relative depth depends on the dimensionless time $t' = t/\tau^*$, $(0 < t' < 1)$ and the dimensionless depth $z' = z/\mathrm{H}$

$$T'(z,t) = \frac{T(z)-T_{av}}{T_o-T_{av}} = \Psi\left\{\frac{z}{H}, \frac{t}{\tau^*}\right\} \text{ (Universal solution C)} \tag{A.10}$$

π_1 in the solution is collected in τ^*.

Sinusoidal temperature at the surface.

For sinusoidal temperature variations on the ground surface, boundary conditions remained the same as well as the mathematical model (Eqs. (1), (2b) and (3)). The characteristic depth or length ($l_{z,o}{}^*$), Fig. 1, have been defined as the depth that is not appreciably affected by the changes of temperature in the surface (for example, 5 or 1 %). The boundary condition at the surface can be split in two parts based on superposition: constant temperature at the surface of value T_{av} - T_o and a harmonic variation of value $\Delta T_{z=0}$. To find the dimensionless groups influence in ΔT for the case of no groundwater flow, we introduce in the governing equation, $k_m\left(\frac{\partial^2 T}{\partial z^2}\right) - c_{e,w}\rho_{e,w}\left(v_{z,o}\frac{\partial T}{\partial z}\right) = 0$, the dimensionless variables defined below:

$$z' = \frac{z}{l_{z,o}{}^*}; t' = \frac{t}{\tau_o}; T' = \frac{T}{\Delta T_{z=0}}$$

where references to make dimensionless such normalized variables are $l_{z,o}{}^*$, τ_o and $\Delta T_{z=0}$. The resulting dimensionless governing equation is

$$\rho_e c_e \frac{\Delta T_{z=0}\partial T'}{\tau_o \partial t'} = k_m \frac{\Delta T_{z=0}\partial^2 T'}{\left(l_{z,o}{}^*\right)^2(\partial z')^2} \tag{A.11}$$

while the only dimensionless group resulting is written as

$$\pi_2 = \frac{\rho_e c_e\left(l_{z,o}{}^*\right)^2}{k_m\tau_o} = \frac{\left(l_{z,o}{}^*\right)^2}{\alpha\tau_o} \tag{A.12}$$

This group provides the order of magnitude of $l_{z,o}{}^*$:

$l_{z,o}{}^* \sqrt{\alpha\tau_o}$

The proportionality constant, obtained by an only numerical simulation, is 1.67, so that

$$l_{z,o}{}^* = 1.668\sqrt{\alpha\tau_o} \tag{A.13}$$

In shallow aquifers in which the total depth is less than $l_{z,o}{}^*$ (that is, the wave amplitude is not negligible at any depth), the depth of the aquifer itself becomes a relevant magnitude and can be used as a reference to make dimensionless , $z' = z/H$. This leads to the dimensionless governing equation $\rho_e c_e \frac{\Delta T_{z=0}\partial T'}{\tau_o \partial t} = k_m \frac{\Delta T_{z=0}\partial^2 T'}{(H)^2(\partial z')^2}$ and to an only group $\pi_2 = \frac{\rho_e c_e H^2}{k_m\tau_o} = \frac{H^2}{\alpha\tau_o}$ on which all harmonic type solutions depend.

The amplitude ΔT_z at each depth is given by:

Thermal deep aquifers: $(H > l_{z,o}{}^*)$:

$$(\Delta T')_z = \frac{(\Delta T)_z}{(\Delta T)_{z=0}} = \Psi\left(\frac{z}{l_{z,o}{}^*}\right) = \Psi\left(\frac{z}{\sqrt{\alpha\tau_o}}\right) \text{ (Universal solution D)} \tag{A.14}$$

Thermal shallow aquifers $(H < l_{z,o}{}^*)$:

$$(\Delta T')_z = \frac{(\Delta T)_z}{(\Delta T)_{z=0}} = \Psi\left(\frac{H^2}{\alpha\tau_o}, \frac{z}{H}\right)\left(\text{Universal solution E}\right) \tag{A.15}$$

In aquifers with vertical groundwater flow, assuming sinusoidal variations at the ground surface, the dimensionless variables of depth, time and temperature are defined as

$$z' = \frac{z}{l_{z,o}{}^*}; t' = \frac{t}{\tau_o}; T' = \frac{T-T_{av}}{\Delta T}$$

Introducing them in Eq. (1), yields

$$k_m \frac{(T_o-T_{av})\partial^2 T'}{\left(l_{z,o}{}^*\right)^2(\partial z')^2} - v_{z,o}\rho_{e,w}c_{e,w}\frac{(T_o-T_{av})\partial T'}{l_{z,o}{}^*\partial z'} = \rho_e c_e \frac{(T_o-T_{av})\partial T'}{\tau_o \partial t'} \tag{A.16}$$

The coefficients or addends of this equation, once simplified, $\frac{\rho_e c_e}{\tau_o}$, $\frac{k_m}{\left(l_{z,o}^{*}\right)^2}$, and $\frac{v_{z,o}\rho_{e,w}c_{e,w}}{l_{z,o}^{*}}$ give rise to two monomials

$\pi_3 = \frac{\rho_e c_e \left(l_{z,o}^{*}\right)^2}{k_m \tau_o} = \frac{\left(l_{z,o}^{*}\right)^2}{\alpha\tau_o}$ and $\pi_4 = \frac{k_m}{\left(l_{z,o}^{*}\right)^2}\frac{l_{z,o}^{*}}{v_{z,o}\rho_{e,w}c_{e,w}} = \frac{k_m}{l_{z,o}^{*} v_{z,o}\rho_{e,w}c_{e,w}} = \frac{\alpha_c}{l_{z,o}^{*} v_{z,o}}$ (A.17).

The physical meaning of these monomials are: π_3 the balance between storage and diffusion and π_4 the balance between diffusion and advection. Removing the characteristic length ($l_{z,o}^{*}$) from one of them, they are reduced to two other equivalent groups (one of them without the unknown $l_{z,o}^{*}$) of the form

$$\pi_5 = \frac{\rho_e c_e \left(l_{z,o}^{*}\right)^2}{k_m \tau_o} = \frac{\left(l_{z,o}^{*}\right)^2}{\alpha\tau_o} \tag{A.18}$$

$$\pi_6 = \pi_{l_{z,o}^{*}} = \frac{\left(l_{z,o}^{*}\right)^2}{\alpha\tau_o}\left(\frac{k_m}{l_{z,o}^{*} v_{z,o}\rho_{e,w}c_{e,w}}\right)^2 = \frac{k_m^{\,2}}{\alpha\tau_o\left(v_{z,o}\rho_{e,w}c_{e,w}\right)^2} = \frac{\alpha}{\tau_o v_{z,o}^{\,2}}\left(\frac{\rho_e c_e}{\rho_{e,w}c_{e,w}}\right)^2 \tag{A.19}$$

So, for thermal deep aquifers ($H > l_{z,o}^{*}$):

$l_{z,o}^{*} = \sqrt{\alpha\tau_o}\Psi\left\{\frac{\alpha}{\tau_o v_{z,o}^{\,2}}\left(\frac{\rho_e c_e}{\rho_{e,w}c_{e,w}}\right)^2\right\}$ (Universal solution F) (A.20).

with f an undetermined function that modulates the solution $l_{z,o}^{*} = \sqrt{\alpha\tau_o}$ ($v_{z,o} = 0$) due to the existence of vertical flow. This dependence is valid both for upward and downward flow. In the non-restrictive case that $\rho_{e,w}c_{e,w} = \rho_e c_e$, the previous expression reduces to

$$l_{z,o}^{*} = \sqrt{\alpha\tau_o}\Psi\left\{\frac{\alpha}{\tau_o v_{z,o}^{\,2}}\right\} \tag{A.21}$$

Applying the pi theorem, the solutions of the unknown $\Delta T' = \frac{(\Delta T)_z}{(\Delta T)_{z=0}}$, both for upward and downward flow are:

Thermal deep aquifers ($H > l_{z,o}^{*}$):

$$\frac{(\Delta T)_z}{(\Delta T)_{z=0}} = \Psi\left(\frac{z}{l_{z,o}^{*}}\right) \text{ (Universal solution G)} \tag{A.22}$$

As regards thermal shallow aquifers, there is no characteristic length within the domain, so that H is introduced instead of $l_{z,o}^{*}$ to non-dimensionalize the independent variable z. In this case the solution for $\Delta T'$, besides their dependence on π_5, depends on the relative position z/H.

Thermal shallow aquifers, $H < l_{z,o}^{*}$:

$$\frac{(\Delta T)_z}{(\Delta T)_{z=0}} = \Psi\left(\frac{z}{H}, \frac{H^2}{\alpha\tau_o}, \frac{\alpha}{\tau_o v_{z,o}^{\,2}}\left(\frac{\rho_e c_e}{\rho_{e,w}c_{e,w}}\right)^2\right) \text{ (Universal solution H)} \tag{A.23}$$

References

Alhama, I., García-Ros, G., González-Alcaraz, M.N., Álvarez-Rogel, J., 2022. Long-term artificial seawater irrigation as a sustainable environmental management strategy for abandoned solar salt works: The case study of Agua Amarga salt marsh (SE Spain). Catena 217, 106429.

Alhama Manteca, I., 2013. Simulation and consequences of successive anthropogenic activity in the Agua Amarga coastal aquifer (southeast Spain). Hydrol. Sci. J. 58 (5), 1072–1087.

Alhama, I., Soto Meca, A., Alhama, F., 2012. Simulation of flow and solute coupled 2-D problems with velocity-dependent dispersion coefficient based on the network method. Hydrol. Process. 26 (24), 3725–3735. https://doi.org/10.1002/hyp.8457.

Anderson, M.P., 2005. Heat as a ground water tracer. Groundwater 43 (6), 951–968. https://doi.org/10.1111/j.1745-6584.2005.00052.x.

Bejan, A., 2013. Convection heat transfer, 4th ed. New York, NY, USA, John Wiley & sons.

Bredehoeft, J.D., Papadopulos, I.S., 1965. Rates of vertical groundwater movement estimated from the Earth's thermal profile. Water Resour. Res. 1 (2), 325–328. https://doi.org/10.1029/WR001i002p00325.

Buckingham, E., 1914. Illustrations of the use of dimensional equations. In: On Physically Similar Systems, p. 6.

Cánovas, M., Alhama, I., Alhama, F., 2015a. Mathematical characterization of Bénard-type geothermal scenarios using discriminated non-dimensionalization of the governing equations. Int. J. Nonlinear Sci. Numerical Simulation 16 (1), 23–34. https://doi.org/10.1515/ijnsns-2014-0068.

Cánovas, M., Alhama, I., Trigueros, E., Alhama, F., 2015b. Numerical simulation of Nusselt-Rayleigh correlation in Bénard cells. A solution based on the network simulation method. Int. J. Numer. Meth. Heat Fluid Flow 25 (5), 986–997.

Cartwright, K., 1979. Measurement of fluid velocity using temperature profiles: experimental verification. J. Hydrol. 43 (1–4), 185–194. https://doi.org/10.1016/0022-1694(79)90172-0.

Duque, C., Müller, S., Sebok, E., Haider, K., Engesgaard, P., 2016. Estimating groundwater discharge to surface waters using heat as a tracer in low flux environments: the role of thermal conductivity. Hydrol. Process. 30 (3), 383–395. https://doi.org/10.1002/hyp.10568.

Ferguson, G., Woodbury, A.D., 2005. The effects of climatic variability on estimates of recharge from temperature profiles. Groundwater 43 (6), 837–842.

Gordon, R.P., Lautz, L.K., Briggs, M.A., McKenzie, J.M., 2012. Automated calculation of vertical pore-water flux from field temperature time series using the VFLUX method and computer program. J. Hydrol. 420, 142–158.

Hatch, C. E., Andrew, F. T., Revenaugh, J. S., Constantz, J., Ruehl, C. R., Los Huertos, M., & Shennan, C. (2002, December). Time-Series Analysis of Streambed Thermal Records to Model Surface Water-Groundwater Interaction Within a Coastal Watershed. In *AGU Fall Meeting Abstracts* (Vol. 2002, pp. H61A-0747).

Hatch, C.E., Fisher, A.T., Revenaugh, J.S., Constantz, J., Ruehl, C., 2006. Quantifying surface water–groundwater interactions using time series analysis of streambed thermal records: Method development. Water Resour. Res. 42 (10).

Healy, R.W., 2008. Simulating water, solute, and heat transport in the subsurface with the VS2DI software package. Vadose Zone J. 7 (2), 632–639.

Healy, R.W., Ronan, A.D., 1996. Documentation of computer program VS2DH for simulation of energy transport in variably saturated porous media—Modification of the US Geological Survey's computer program VS2DT. Water-Resources Investigations Report 96, 4230.

Irvine, D.J., Lautz, L.K., Briggs, M.A., Gordon, R.P., McKenzie, J.M., 2015. Experimental evaluation of the applicability of phase, amplitude, and combined methods to determine water flux and thermal diffusivity from temperature time series using VFLUX 2. J. Hydrol. 531, 728–737.

Jensen, J.K., Engesgaard, P., 2011. Nonuniform groundwater discharge across a streambed: heat as a tracer. Vadose Zone J. 10 (1), 98–109. https://doi.org/10.2136/vzj2010.0005.

Jiménez-Valera, J.A., Alhama, F., 2022. Dimensionless characterization to estimate horizontal groundwater velocity from temperature-depth profiles in aquifers. Mathematics 10 (15), 2717. https://doi.org/10.3390/math10152717.

Keery, J., Binley, A., Crook, N., Smith, J.W., 2007. Temporal and spatial variability of groundwater–surface water fluxes: Development and application of an analytical method using temperature time series. J. Hydrol. 336 (1–2), 1–16.

Kurylyk, B.L., Irvine, D.J., Bense, V.F., 2019. Theory, tools, and multidisciplinary applications for tracing groundwater fluxes from temperature profiles. Wiley Interdiscip. Rev. Water 6 (1), e1329.

Lapham, W.W. (1989). *Use of Temperature Profiles Beneath Streams to Determine Rates of Vertical Ground-Water Flow and Vertical Hydraulic Conductivity*; Paper 2337; U.S. Geological Survey Water-Supply: Reston, VA, USA. https://doi.org/10.3133/wsp2337.

Lautz, L.K., 2012. Observing temporal patterns of vertical flux through streambed sediments using time-series analysis of temperature records. J. Hydrol. 464, 199–215. https://doi.org/10.1016/j.jhydrol.2012.07.006.

Lin, Y.F., Chang, C.H., Tsai, J.P., 2022. Analytical solution for estimating transient vertical groundwater flux from temperature-depth profiles. J. Hydrol. 610, 127920.

Lu, N., Ge, S., 1996. Effect of horizontal heat and fluid flow on the vertical temperature distribution in a semiconfining layer. Water Resour. Res. 32 (5), 1449–1453. https://doi.org/10.1029/95WR03095.

Meca, A.S., Alhama, F., Fernandez, C.G., 2007. An efficient model for solving density driven groundwater flow problems based on the network simulation method. J. Hydrol. 339 (1–2), 39–53. https://doi.org/10.1016/j.jhydrol.2007.03.003.

Network, H.J., Method, S., 2002. Research Signpost: Trivandrum. Kerala, India.

PSPICE, "version 6.0: Microsim Corporation." 20 Fairbanks, Irvine, California 92718, 1994.

Schmidt, C., Conant Jr, B., Bayer-Raich, M., Schirmer, M., 2007. Evaluation and field-scale application of an analytical method to quantify groundwater discharge using mapped streambed temperatures. J. Hydrol. 347 (3–4), 292–307.

Sebok, E., Duque, C., Kazmierczak, J., Engesgaard, P., Nilsson, B., Karan, S., Frandsen, M., 2013. High-resolution distributed temperature sensing to detect seasonal groundwater discharge into Lake Væng, Denmark. Water Res. Res. 49 (9), 5355–5368. https://doi.org/10.1002/wrcr.20436.

Seco-Nicolás, M., Alarcón, M., Alhama, F., 2018. Thermal behaviour of fluid within pipes based on discriminated dimensional analysis. An improved approach to universal curves. Appl. Therm. Eng. 131, 54–69. https://doi.org/10.1016/j.applthermaleng.2017.11.091.

Silliman, S.E., Ramirez, J., McCabe, R.L., 1995. Quantifying downflow through creek sediments using temperature time series: one-dimensional solution incorporating measured surface temperature. J. Hydrol. 167 (1–4), 99–119.

Stallman, R.W., 1963. Computation of groundwater velocity from temperature data. US. *Geol. Surv. Water Supply Pap.* 1544, 36–46.

Stallman, R.W., 1965. Steady one-dimensional fluid flow in a semi-infinite porous medium with sinusoidal surface temperature. J. Geophys. Res. 70 (12), 2821–2827. https://doi.org/10.1029/JZ070i012p02821.

Suzuki, S., 1960. Percolation measurements based on heat flow through soil with special reference to paddy fields. J. Geophys. Res. 65 (9), 2883–2885.

Taniguchi, M., 1993. Evaluation of vertical groundwater fluxes and thermal properties of aquifers based on transient temperature-depth profiles. Water Resour. Res. 29 (7), 2021–2026.

Turcotte, D.L., Schubert, G., 1982. Geodynamics: Applications of Continuum Physics to Geological Problems. John Wiley & Sons, New York.

Ziagos, J.P., Blackwell, D.D., 1986. A model for the transient temperature effects of horizontal fluid flow in geothermal systems. J. Volcanol. Geoth. Res. 27 (3–4), 371–397.